Analytical Model and Experimental Testing of the Limits of Hydraulic Fracture Caging

Luke P. Frash[1]*, Meng Meng[1]*, and Wenfeng Li[1,2]*

[1] Los Alamos National Laboratory, Los Alamos, NM, USA.

[2] New Mexico Institute of Mining and Technology, Socorro, NM, USA.

* All authors contributed equally to this work.

Corresponding author: Luke P. Frash (lfrash@lanl.gov)

Key Points:

1. Fracture caging uses boundary wells to limit fluid-driven fracture growth and to contain flow in hydropropped fractures
2. Fracture caging fails if production rates are too constricted or if fractures do not intersect boundary wells
3. Fracture caging can be achieved with as few as two boundary wells, but three or more wells increases stability

Abstract

Enhanced Geothermal Systems (EGS) are a promising concept for unlocking the great potential of Hot Dry Rock (HDR) resources for clean and sustainable energy production. It can be argued that three of the foremost unsolved challenges for EGS are: induced seismicity, uneconomically low flow rates, and premature cooling of the produced fluid. We propose that fracture caging could be a solution to these three challenges. Fracture caging is the placement of a ‘cage’ of boundary wells around injection wells before fluid stimulation or circulation begins. This fracture cage is intended to contain injected fluids and to thereby limit fracture growth. In the long term, this fracture cage permits sustained high-pressure fluid injection to hold fractures open using hydraulic pressure (i.e., ‘hydropropping’) instead of by using proppant particles or by shear asperity propping. In this study, we present an analytical model and laboratory experiments that quantitatively explore the limits of tensile hydraulic fracture caging. Discoveries from this work include: (1) the maximum flow rates that can be caged are limited by flow constrictions in the boundary wells but are not limited by the injection pressure, (2) a hydraulic fracture can be caged with as few as two boundary wells, and (3) tensile fractures can be hydropropped without growing larger during sustained high-pressure fluid injection into a cage.

Plain Language Summary

Geothermal energy is entering a new frontier where power plants that can generate electricity using the heat of the Earth will no longer be limited to rare high-grade resources. The key issues holding back deployment are well established: (1) typical hot rock resources lack water for energy production, (2) engineering rock to accommodate the flow rates for needed for power production is not trivial, (3) the hot rock must be accessed by costly wells, and (4) geothermal systems pose a risk for triggering earthquakes. In this paper, we present our most recent research to investigate a new approach to geothermal resource development that we call ‘fracture caging’. At its core, fracture caging merely asks for boundary wells to be drilled in a circle around future water injection wells. Our work demonstrates that this up-front investment provides a reliable solution to contain fluid flow. This permits injection and extraction rates can be set to the most optimal values for economic power generation. Likewise, this cage should be able to contain triggered earthquake risk. Our work is a pioneering step towards enabling enhanced geothermal energy to unlock the frontier of clean geothermal energy anywhere.

1 Introduction

Geothermal resources can provide sustainable clean baseload energy for industrial, commercial, and residential uses. Increased use of geothermal energy will help to reduce carbon emissions for climate change mitigation and it will be a key component of the energy transition away from fossil fuels. Despite these benefits, geothermal energy is underutilized in practice. According to a U.S. Department of Energy report, the maximum rated output capacity of geothermal energy production in the United States was only 3.7 GWe in 2019, which could be increased to 60 GWe by 2050 once the technical barriers, including induced seismicity and poor economics, are properly addressed [Hamm et al., 2019].

Enhanced Geothermal Systems (EGS) have the most potential for growth because, unlike a conventional hydrothermal system, EGS do not require abundant in-situ water nor do they require permeable rock [Hamm et al., 2019]. The EGS concept is typically envisioned as a well doublet with one well for water injection and the other for production. This vision assumes that flow is established by creating new fractures or reactivating preexisting fractures in geothermal reservoirs [Tester et al., 2006; Kelkar et al., 2016]. However, there are some outstanding technical problems that hinder unlocking the great potential of EGS. First, fluid injection induced seismicity has been identified as a major threat [Cuenot et al., 2008; Catalli et al., 2013; Ellsworth, 2013]. For example, a Mw 5.7 earthquake has been linked to at an EGS pilot site in Pohang, South Korea [Kim et al., 2017] even though state-of-the-art mitigation methods were employed. These methods included cyclic soft stimulation, the so-called traffic light system, and real-time seismic monitoring. Second, high-rate and high-pressure water injection is often required to achieve economic power production from EGS [Petty et al., 2013; Garcia et al., 2016]. Exiting seismicity mitigation measures impose limits on injection rates and pressures with the goal of reducing seismic risk, but paradoxically no methods yet exist to predict what these limits should be for a given site. To be fair, the theory is understood for how such limits could be predicted, but the reality is that we lack the required input data to parameterize these predictive models. Third, short circuited flow of water between injection and production wells is common. Short circuiting is when the working fluid preferentially flows along a single path, as opposed to a multiple paths, which in turn results in a low effective surface area for heat extraction. This leads to premature cooling of the produced fluid and inefficient utilization of the hot rock resource. These short circuits are inevitable due to fracture heterogeneity and fluid-rock interactions at elevated temperatures that promote flow channeling [André et al., 2006; Pruess, 2008; Gee et al., 2021. Solutions to prevent short circuiting are practically limited to in-well zonal flow control tools and techniques. Research and the development of new technologies are required to address these technical problems.

Recently, we introduced the concept of ‘fracture caging’ to limit induced seismicity and to enable sustained high-rate high-pressure fluid circulation [Frash et al., 2018 & 2021]. Fracture caging involves boundary wells surrounding an injection well to proactively limit fracture stimulation and achieve fluid flow containment in a geothermal reservoir. However, our prior work did not investigate the limits of fracture caging because the experiments were too short in duration to confirm halting of fracture growth, did not investigate the minimum number of boundary wells that could cage a hydraulic fracture, and did not identify the parameters that control the maximum flow rate that can be caged. Here, we will rectify these shortcomings and will demonstrate that fracture caging holds promise for field-scale application.

To elaborate on fracture caging and the motivations for studying it, we hypothesize that fracture caging has the potential to solve the three foremost technical challenges related to EGS viability: (1) induced seismicity that can damage nearby structures, (2) excessively low flow rates that preclude economic power generation, and (3) thermal short circuiting that leads to premature cooling of the produced fluid. To confront seismicity, controlling fracture growth and achieving fluid containment using fracture caging offers the means to limit the length of fracture slip, thus controlling the maximum magnitude of seismicity [Kanamori and Anderson, 1975]. To confront low flow rates, EGS requires long-term fluid injection at high-rate and high-pressure without the typically expected increase to seismic risk [Jeanne et al., 2015]. Fracture caging could decouple flow rate and pressure from seismic risk, removing the need for flow limits. To confront thermal short circuiting, increased active fracture surface area and a uniform flow sweep without channeling is required. Fracture caging opens the possibility of propping fractures open with high-pressure fluid which could mitigate the severe flow channeling caused by heterogeneous closed areas in fractures. When this tensile opening occurs without fracture growth, we refer to this condition as ‘hydropropping’ because the high-pressure fluid is the proppant. With hydropropping neither solid sand proppant nor shear propping would be required to maintain hydraulic conductivity. In addition, the removal of pressure limits using caging will increase options for in-well tools for long-term flow control, such as limited entry casing perforations [Frash, 2022].

Our recently proposed concept of fracture caging requires more development and validation before it can be confidently applied. A crucial next step is to conduct experiments to validate the ability of fracture caging to halt fracture growth during sustained high-rate high-pressure flow. Previous experiments were too breif to be conclusive on in this regard. By extension, proof of stable hydropropping is also needed. The premise of drilling multiple boundary wells is an economic deterrent against using caging, so models and experiments are needed to investigate the minimum number of boundary wells that can cage an active fracture. In this modeling and experimental study, we present an analytical model to predict the maximum flow rate that can be caged at any scale and we present a series of new laboratory experiments to evaluate the performance of fracture caging in three, four, and five well geometries. In addition to verifying the ability of boundary wells to halt fracture growth, these lab experiments tested hydropropped fracture stability across a range of flow rates and a range of open versus closed configurations for the boundary wells. With the inclusion of acoustic emission measurements, these experiments provide a rich dataset with applications beyond our interest area. Ultimately, we will prove that a hydraulic fracture can be halted by as few as two wells, that larger fractures are easier to cage than smaller fractures, that the maximum caged flow rate is primarily a function of well diameter, and that stable hydropropped fractures are possible even when the injection pressure exceeds the static pressure required for fracture growth.

2 Fracture Caging Analytical Model

In this section we present our conceptual model for how fracture caging can be achieved in fractures of any size. We begin with a simple model to estimate fracture radius as a function of cumulative injected volume. Next, we consider frictional flow effects to predict caged fracture stability as a function of injection rate. The geometry, fluid properties, and material properties used in this section are consistent with those used for our experiments. Ultimately, our results indicate that caging should be possible in commercial geothermal systems.

2.1 Fracture radius from injected volume

We require a model to predict uncaged fracture radius as a function of injected fluid volume in order to verify that caging can halt hydraulic fracture growth. Later, we will use this model to compare predicted uncaged radii to measured caged radii. We start with the same homogeneous, elastic, impermeable, Newtonian fluid, and laminar flow assumptions that are used by many analytical hydraulic fracture models. These assumptions will be met in our experiments by using acrylic as our host material and oil as our fluid. Next, we must point out that existing analytical hydraulic fracture models were created to predict hydraulic fracture radius and net pressure as a function of a constant injection rate and time [Detournay, 2004]. In the case of fracture caging, these existing models can only be applied up until when the fracture first intersects a boundary well. After this time, fluid is both being injected and produced so volume balance is no longer controlled solely by the injection parameters. Consequently, existing hydraulic fracture growth models are not directly applicable to fracture caging. Instead, we will assume that the fracture is caged at a constant radius with steady-state hydropropping and uniform net pressure. This permits the use of Sneddon's equation [Sneddon and Lowengrub, 1969] to estimate the aperture (*w*) at the center of an elliptical penny-shaped tensile hydraulic fracture as a function of radius (R_f) with its uniform net pressure at the critical limit for propagation (P_c).

$$w = \frac{8P_c(1-v^2)R_f}{\pi E} \tag{1}$$

The Young's modulus (*E*) and Poisson's ratio (*v*) for acrylic can be taken as 2.6 GPa and 0.40, respectively. Since the fracture geometry is elliptic, we can estimate the volume (*V*) of this fracture directly from the radius (R_f) and center-point aperture (*w*). Rearranging, we can now estimate the fracture radius as a function of the cumulative injected fluid volume.

$$V = \frac{2\pi {R_f}^2 w}{3} \tag{2}$$

$$R_f = \sqrt[3]{\frac{3VE}{16P_c(1-v^2)}} \tag{3}$$

Many analytical solutions to predict critical fracture pressure (P_c) and dimensions (*w*, R_f) have been proposed, such as by using linear-elastic-fracture-mechanics [Valko and Economides, 1996] or by using both flow and fracture mechanics [Detournay, 2016]. These solutions require material parameters such as fracture toughness which are notoriously difficult to measure. However, in our case, we have the advantage of measuring the critical fracture pressure in the same material, using the same fluid, and at the same dimensions as our experiments. Later, we will detail our measurements of this value (P_c) at 2.3 ±0.1 MPa.

2.2 Caging injection rate limit

Let us consider pressure losses with flow through a hydropropped fracture that is maintained at the critical limit for fracture propagation (P_c). Again, our experiments will show this value to be 2.3 ±0.1 MPa in acrylic. The flow rate that is needed to induce this critical pressure in a caged and hydropropped fracture will be the maximum rate that can be caged. Further, a caged fracture includes simultaneous injection and production at equal total rate. Ideally, the total production rate will be equally split among all production wells. Here, we will not attempt to account for how fracture heterogeneity and flow instability will result in non-equal flow distribution. The frictional flow terms that are most likely to control caged fracture flow inside an arbitrarily shaped fracture include: (ΔP_x; Eq. 4; Jeppson, 1974) pressure losses with flow through the wells, (ΔP_r; Eq. 5; Yen, R.T., 1962) pressure losses with flow through the near-wellbore zone, (ΔP_l; Eq. 6; Witherspoon et al., 1980) pressure losses with flow through narrow fractures, and (P_p) the backpressure at the outlet of the boundary wells.

$$\Delta P_x = \frac{1.14\times10^8 Q^{1.852}\mu x}{f^{1.852}(2R_w)^{4.87}} \tag{4}$$

$$\Delta P_r = \frac{6Q\mu \ln{(r/R_w)}}{\pi h^3} \tag{5}$$

$$\Delta P_l = \frac{12Q\mu l}{Hh^3} \tag{6}$$

Where, Q is volumetric flow rate, μ is fluid viscosity, l is flow path length, H is flow path height or width, h is hydraulic aperture, R_w is well radius, f is pipe roughness, and x, r, and l are distances along the flow line. Rough pipe has an f value of around 80. Standard units for the above equations are m, s, and Pa. Without assuming specific well locations within a fracture, we will estimate fracture net pressure using total hydraulic force (F) over the respective area of the fracture (A).

$$P_c = \frac{F}{A} \tag{7}$$

$$F = \sum \int (\Delta P_i + P_{io})dx \tag{8}$$

Where i is the flow element (e.g., well, near-well, or fracture) and io is the pressure downstream of this element. The only element that will not influence the ability to cage the fracture is the pressure loss through the injection well because the fracture's net pressure is a consequence of the downstream losses. To account for fracture stranding (i.e., multiple fractures, N_f) and multiple boundary wells (N_p), we can impose simple division if we assume an equal distribution of flow.

$$Q_{pro} = \frac{Q_{inj}}{N_p} \tag{9}$$

$$h = \frac{w}{N_f} \tag{10}$$

Given a fracture radius, well diameter, and well spacing, this system of equations can be solved to calculate the injection rate limit for a caged hydraulic fracture. Our solution is provided in our online data repository (https://zenodo.org/record/8274273). To aid upscaling, we will take a constant ratio of 0.75 between the well spacing and fracture radius. Also, we will take the radius of influence of the near well zone to be 1/6th of the well spacing. For well length, we use a ratio of 2 with respect to the well spacing. These ratios ensure that crucial flow constricting processes are accounted for, and the ratios allow us to evaluate caging at small and large scales by varying the well spacing and well diameter (Fig. 1). This model predicts that fracture caging is possible at the lab scale (i.e., 1 to 100 cm) and the field scale (i.e., 100 to 1000 m). At field scales, the maximum injection rate (Q_{inj}) that can be caged is predicted to be primarily a function of the well diameter due to the backpressure that builds from flow through the production well (Q_{pro}). The model also predicts that caging becomes easier as the fracture grows with a given well spacing because longer fractures will have larger apertures, lower near-well pressure losses, and lower in-fracture pressure losses.

3 Experiment Description

Hydraulic fracture caging laboratory experiments were conducted using high viscosity oil injection into blocks of acrylic. Each block contained one central injection well surrounded by two or more boundary wells (Fig. 2). The boundary wells were pre-drilled before injection so that they could cage an approaching hydraulic fracture during the stimulation process. Once a hydraulic fracture became caged by these boundary wells, as would be indicated by halting of fracture growth, the boundary wells would continue to serve the role of production wells (i.e., producers) during experimentation with hydropropping. Collectively, these experiments for fracture caging investigated the effects of facture orientation, the number of boundary wells during stimulation, the number of active producers during hydropropping, injection rates, and boundary well flow control methods.

3.1 Experimental setup

Polymethyl methacrylate (i.e., PMMA or acrylic) was selected for our experiments primarily because it is transparent which allows close observation of hydraulic fracturing and fluid circulation. Beneficially, this material has extremely low permeability, is non-porous, has a tendency toward brittle fracture, and its deformation can be described as elastic dominated.

These properties eliminate undesirable complexities, such as diffusive flow, while retaining the ability to unambiguously measure hydraulic fracture radius due to its transparency.

The injection fluid was high-viscosity oil with red dye to enhance visibility. At 20° C room temperature, this oil has a viscosity of 404 cP. Combining this with our targeted stimulation rate of 0.5 mL/min, estimated duration of at least 1.0 s, and fracture toughness of 1.55 MPa-m2 [Weerasooriya, 2006], it can be shown that this yields toughness-dominated hydraulic fracture growth [Detournay, 2004]. Based on our experience, using this oil slows fracture propagation enough for standard 60 fps video to observe growth at the laboratory scale.

Wells were drilled into each acrylic block using the design shown in Fig. 2. The upper portion of each well was sealed using stainless steel tubing and epoxy. The lower portions of the wells were open-hole (i.e., no casing). The center well was notched with a 45° circular plunge cut to a depth of 0.16 cm to guide hydraulic fractures into a transverse orientation. Well spacing was constant as the number of boundary wells was set at either 2, 3 or 4, with separation angles of 180°, 120°, and 90° respectively. Outside the blocks, 0.152 cm inner diameter (i.e., 1/8”) stainless steel tubing with a nominal length of 200 cm connected each well to its own syringe pump.

Digital cameras were used to record video of the fracture throughout each experiment. Blocks were unconfined to allow visual observation. Although external polyaxial stresses are known to be important and possible to simulate in the laboratory [Frash et al., 2015; Hu and Ghassemi, 2017], such approaches do not allow the visual observation of fracture growth that we require to unambiguously confirm fracture caging. Conveniently, notches, such as ours, can be used to orient hydraulic fractures in the laboratory when applied stresses are negligible.

Threshold triggered acoustic emissions (AE) were monitored throughout all experiments. A total of 8 piezoelectric sensors were epoxied to the surfaces of each sample. The sample, the AE sensors, and wiring were all shielded in a metal cabinet to minimize noise. Each AE sensor had a resonant frequency of 2.1 MHz by thickness and 196 kHz by diameter. While it is possible to perform source location and deconvolution with our data [Ohtsu, 1991 & 1995], here we employ AE only for event counting.

3.2 Experimental procedures

Our experiments were conducted in four phases: ‘hydraulic fracturing’, ‘fluid circulation’, ‘flow heterogeneity’, and ‘critical pressure’. Details follow and any exceptions are detailed in the experiment results section.

The ‘hydraulic fracturing’ phase used a constant injection rate to induce a fluid driven fracture in our notched central injection well. While care was taken to bleed all air from injection pump, the boundary wells were either: (C1) bled of air and configured to actively maintain backpressure using servo-mechanical motors or (C2) they were filled with 50 mL of air to serve as a passive pressure accumulator. For the first control mode (C1), the backpressure was set at 0.5 MPa which was the minimum control setpoint. This control response was slow, but enabled production rate measurement. For the second control mode (C2), the backpressure was atmospheric at 0.77 atm due to the 2220 m elevation of our facility. This (C2) control response was immediate to minimize pressures surges. These details will be shown to be crucial for caging.

The ‘fluid circulation’ phase involved multiple stages of continuous oil injection at increased rates and pressures while oil production rates were measured using the active control mode (C2) for the pumps. This process investigated the cage stability and the viability of hydropropping. In other words, whether-or-not a caged fracture could support long-term, high-rate, and high-pressure fluid injection without inducing fracture growth.

The ‘flow heterogeneity’ phase was completed next. Now, the influence of boundary well shut-in (i.e., closure) was investigated by sequentially stopping all but one of the boundary well pumps while continuing fluid injection. This process investigated the robustness of a caged fracture in the event of one or more boundary wells becoming clogged or being taken offline for maintenance. Such events will occur in field applications of fracture caging and hydropropping for EGS.

The ‘critical pressure’ phase was completed after confirming caged hydraulic fracture stability with long-term injection. In this phase, all production was halted while injection continued until fracture growth resumed. This provided the critical pressure (P_c) measurement for our model and it confirmed the ability to resume fracture growth by disabling the fracture cage.

This experiment design was inspired by field observations from the decameter-scale multi-well EGS Collab project [Fu et al., 2021; Meng et al., 2021]. In this project, long-term high-pressure fluid injection was performed and stable hydropropping was suspected due high production rates and a lack of microseismic activity. During this time, the distribution of production was unsteady and heterogenous which indicated issues such as chemical dissolution and precipitation, thermal flow channeling, poromechanical effects, biological growth, flow instabilities, and particulate mobilization and clogging. We imposed heterogeneous fracture flow in our experiments to assess the performance of fracture caging in non-ideal circumstances to provide assurance that caging can be reliably maintained in more complex scenarios.

4 Experiment Results

The main objective of the present study was to demonstrate fracture caging during hydraulic stimulation and during hydropropping with sustained high-pressure fluid circulation. For completeness, we examined situations that led to both caged and uncaged fractures. This enabled us to not only verify that sustained caging and hydropropping are possible, but also to evaluate the limits of fracture caging.

4.1 Caged fracture with four boundary producers

First, we present an experiment where a hydraulic fracture was successfully and stably caged by four boundary producers (Fig. 3). The pressure accumulator control mode (C2) was employed to maximize the chance of successful fracture caging. A hydraulic fracture was induced at a breakdown pressure of 39.5 MPa using injection at 0.5 ml/min. As shown in the images (Fig. 4), the fracture grew rapidly from 0 to 0.012 min (0.72 s) when it first intersected a boundary well with an estimated injected volume of less than 0.1 mL and a nominal radius of 35 mm. Next, injection continued but the fracture grew more slowly until it halted all growth at 0.129 min (7.74 s) with the injected volume now totaling at 2.9 mL and the radius reaching 55 mm. Thereafter, the fracture size remained unchanged at its 55 mm radius until 217 min (13,000 s) despite more than 245 mL being injected at rates of up to 8 mL/min. At this time and if the acrylic block had been larger, the predicted uncaged radius of the fracture would have been 394 mm per Eq. (3). At around 217 min, the finally fracture grew again because fluid was being injected into the boundary well at a rate of up to 20 mL/min without any simultaneous production. In hindsight, the pumps should have been disconnected from the block at this time because this injection was performed merely to purge air from the pumps, so this injection into the block was unintended. Later, growth was intentionally induced at 231 min using injection without production. The only mechanism for halting of fracture growth throughout this process was fracture caging, so this result unequivocally proves that fracture caging can halt fracture growth and that caging can contain high-pressure fluids during long-term injection to enable stable hydropropping.

During fluid circulation, injection pressures reached up to 6.22 MPa which is much higher than the static critical pressure of 2.28 MPa. Meanwhile, the flow rate from each producer was variable, oscillating between 20% and 32% of the injection rate. This indicates flow instability despite the fracture radius remaining constant. The heterogeneous flow tests further investigated this flow instability. To begin, the injection rate was maintained at 2.0 ml/min, one producer was controlled under a constant pressure of 0.25 MPa, and the other three producers were all set an initial constant production rate of 0.5 ml/min. This combination of constant pressure and constant rate control of the four producers improved flow stability. Next, all but one of the producers were sequentially shut-in. The hydraulic facture retained a constant caged length throughout, confirming the possibility of stable hydropropping.

Over the course of this experiment, more than 600 events were recorded. Of these, 38 events were associated with hydraulic fracture breakdown. Additional AE activity was recorded while the boundary pumps were bled of air from 150 to 220 min. AE was also recorded when the fracture propagated at 231 min during the critical pressure stage. While these periods of AE activity did coincide with fracture growth, the results are ambiguous to interpret which highlights the unambiguous value of using transparent acrylic.

4.2 Caged fracture with three boundary producers

Second, we conducted a fracture caging experiment using three boundary producers (Fig. 5). The fracture breakdown pressure was measured at 37.5 MPa with an injection rate of 0.5 mL/min. Just as the four boundary well experiment, the fracture growth was rapid until it intersected the first boundary well at 0.006 min (Fig. 6). The growth then slowed until it halted at 0.181 min, at which time the fracture was now fully caged as verified by continued injection. This injection continued until 139 min when a total volume of 178 mL of oil had been injected. The radius of the fracture up until the critical pressure test at 139 min had remained stable at 46.6 mm, despite the predicted uncaged radius being as large as 355 mm. Injection continued after this critical pressure tests with the new fracture radius of 48.1 mm, ultimately injecting 338 mL which is enough fluid to create an uncaged fracture of 438 mm radius. Notably, the injection pressure at 8 mL/min decreased after the critical pressure test, going from 5.5 MPa to 4.2 MPa. This reduced injection pressure with a larger hydraulic fracture indicates a positive relationship between increasing fracture size and more stable caging. Our model agrees with this observation by predicting higher caged injection rate limits when the fracture is larger. Just as the four boundary well experiment, this result again confirmed stable hydraulic fracture caging and stable hydropropping with only three boundary wells.

4.3 Caged fracture with two boundary producers

In the third experiment, the injection borehole was caged by only two boundary producers while the other experiment procedures remained generally the same (Fig. 7). Hydraulic fracture breakdown occurred at 15.7 MPa with injection at 0.5 mL/min and this lower peak pressure coincided with slower fracture growth. In this case, the hydraulic fracture first reached a boundary well at 0.045 min and halted growth due to caging at 0.122 min (Fig. 8). Fracture growth resumed between 15.1 and 17.3 min when the injection rate was increased to 8.0 mL/min despite simultaneous production from the boundary wells. At 17.3 min, a total of 44 mL oil had been injected while the actual caged fracture radius reached 43.8 mm. This radius is being 20% less than the model predicted uncaged radius of 223 mm at this injected volume. At 58.7 min growth resumed again at the injection rate of at 8.0 mL/min, but around this time the fracture was stable at the injection rate of 4 mL/min or less, including during injection at 2 mL/min during the flow heterogeneity stage with one boundary well shut-in. The final growth was observed at 74.3 min during the critical pressure test which measured a respective value of 2.6 MPa for inducing fracture propagation. Interestingly, injection at 8 mL/min was resumed at 90 min but the radius of the fracture remained constant in this time. These results indicate that fracture caging is possible with as few as two boundary wells, but the cage is less stable than what was achieved with three or more boundary wells. For this reason, we conclude that at least three wells is the minimum number of wells needed to reliably cage a hydraulic fracture.

4.4 Uncaged fractures

Our fourth, fifth, and sixth experiments present failed fracture caging scenarios (Fig. 9). These three scenarios all used oil-filled boundary wells with the active servo-mechanical pump pressure control mode (C1). In other words, we expected a slower production rate response time when the hydraulic fracture hits the production wells. This decision was fateful in revealing that fracture caging is most effective when coupled with the ability to rapidly accommodate surge flow. Surge flow is high when the hydraulic fracture first intersects the boundary wells. If we correct the injection rates to account for pump and well elastic ballooning (i.e., pressure dependent injected volume) we observe surge flow rates faster than 40 mL/min in the early stages of hydraulic fracture propagation. This was most apparent in the sixth experiment with its four boundary wells since the transverse hydraulic fracture was able to propagate to the outer edge of the acrylic block despite active production from the boundary wells. This result was unlike the first experiment that used control mode (C2) with its faster flow response which enabled the fracture to be completely caged. Note that this control mode was the only difference between these two experiments since the breakdown pressure was nearly identical at 39.5 and 38.4 MPa, sequentially. Additionally, in the sixth experiment, pressure rise was observed in all four boundary well pumps with maximum pressures of 0.8, 1.6, 2.5, and 3.1 MPa reached as the four pumps attempted to maintain 0.5 MPa. Collectively, these results demonstrate that caging can fail when the production rate is too constricted, especially during stimulation.

The fourth and fifth experiments demonstrate an altogether different failure mechanism. Both of these experiments used three boundary wells. Both of these experiments failed to induce transverse hydraulic fractures, perpendicular to the injection well. In the fourth experiment, the hydraulic fracture was longitudinal and completely missed the boundary wells. In the fifth experiment, the hydraulic fracture was inclined and intersected only one boundary well. Slowed fracture growth was observed in the fifth experiment, similar to what was observed in the sixth experiment, but the fracture still reached the outer edge of the block because the production rate was too low. The cause of the longitudinal fracturing in these experiments stems from Kirsch stresses and inadequate notching to overcome the tendency for hydraulic fractures to be longitudinal when the applied far-field compressive stresses are low, isotropic, or near-isotropic. This issue is also prevalent in field wells for the same reasons, but the stress anisotropy can exceed 10 MPa, which helps steer fractures perpendicular to the minimum principal stress.

A keen eye will notice that experiments five and six included oil injection after the hydraulic fracture cage had failed and reached the outer edge of the block. This injection was performed to evaluate fluid containment by fracture caging when the hydraulic fracture growth is uncontained. The recovery rates in these cases ranged from 11 to 42% of the injected fluid. Higher recovery rates were achieved at lower injection rates. More fluid was able to be recovered when more boundary wells were intersected. This result demonstrates that caging can see partial success when the fractures are uncontained but the lowest resistance leak paths will still dominate. In this case, the flow path from the injection well to the outer edge of the block at its 0 MPa gauge pressure provided much less flow resistance than flow from the injection well to the boundary wells which each imposed 0.5 MPa backpressure. Actually, it is remarkable that the recovery rates could even be as high as 42% when the fracture was not caged.

5 Discussion

This study focuses on fracture caging in homogeneous, elastic, and impermeable material. We must acknowledge that uncertainties at a geothermal site, such as rock heterogeneity, in-situ stress variation, and complex natural fractures, are key factors that could greatly affect the performance of a fracture cage. While we continue to pursue studies of these complexities, we also hope that the work presented here serves to motivate others in the community to investigate the potential of fracture caging in more complex and realistic scenarios. With luck, it may turn out that fracture caging, or some variant of this concept, could help to unlock more than 60 GWe of clean power generation in the United States [Hamm et al., 2019], and even more globally. Our study demonstrates that such an effort could be worthwhile as the scientific community explores the concept of fracture caging for subsurface flow containment and injection induced seismicity control.

In the beginning of this paper, we claimed that fracture caging could be a solution to the grand challenges of EGS that include: (1) limiting induced seismicity, (2) increasing flow rates, and (3) delaying cooling. The results in this study do support this claim, but in a non-obvious way.

To elaborate on seismicity control (1), our results unequivocally prove that boundary wells can contain fracture growth and they can enable stable hydropropping. This implies that the lengths of hydraulically activated fractures can be controlled using caging. While uncertainties do persist with respect to the mechanics of fluid injection into critically stressed faults [Ito and Zoback, 2000; Zoback and Gorelick, 2012; Galis et al., 2017] and its connection to caging the maximum seismic magnitude [Frash et al., 2021], the basic premise that limiting the volume of perturbed rock should reduce seismicity is logical. Here, we presented a model and experimental evidence for the concept that fracture caging can limit the volume of perturbed rock by halting hydraulic fracture growth and by containing flow in hydropropped fractures. Therefore, our evidence that caging can contain the perturbed volume of rock during high-rate, high-pressure, long-term fluid injection is also evidence that caging should be able to limit induced seismicity.

With respect to increasing permissible flow rates (2), standard seismicity mitigation procedures [Majer et al., 2012] seek to limit seismic risk by imposing injection pressure and flow rate limits. Unfortunately, these limits they tend to cause EGS to become uneconomic, especially when the realized injection pressures happen to be higher than what was hoped for during project planning. Economic flow for EGS demands controllable rates so that heat extraction can be optimized for maximum power generation over the lifespan of the well. Conventional solid particle proppants may be able to help reduce injection pressures and increase achievable flow rates, but the stability of proppants in the long term is unlikely due to crushing, embedment, and chemical dissolution. The next alternative is shear asperity propping where existing shear fractures and faults are used to provide flow conduits. If the permeability of these features is low, but not too low, medium-pressure fluid injection offers the chance to enhance permeability through shear stimulation. However, high-performance shear-fracture dominated systems are a Goldilox problem, requiring an improbable, unpredictable, and uncontrollable mix of suitable parameters to come together in order to make EGS economic [Meng et al., 2022]. Also, these shear reliant systems risk large seismic events of 4.0 Mw and greater [Kim et al., 2018]. Compounding the problem, both shear and particle propped fractures will have highly heterogeneous flow [Welch et al., 2022; Katende et al., 2022] while flow in more open fractures tends to be more sheet-like [Petrovich et al., 2013], with sheet-like flow being more ideal for efficient heat extraction [Okoroafor et al., 2022]. Now, we have demonstrated hydropropping as an alternative to shear and solid particle propping. Hydropropping offers sheet-like flow for increased heat recovery efficiency and it effectively removes pressure and flow rate limiters, provided large enough wells are used (Fig. 1). In short, hydropropping could be a solution to safely achieving the high flow rates that EGS needs to be economic.

The link between caging and delayed onset of cooling the produced fluid (3) in EGS is perhaps the least obvious connection. Conveniently, an analytical model was developed that predicts delayed cooling as fluid flows from one well, through fractures, to another well [Gringarten et al., 1975]. This model predicts that larger well spacing, increased flowing surface area, and more fractures will result in a slower onset of produced fluid cooling, assuming the total injection rate is a fixed value. With fracture caging and hydropropping eliminating injection pressure limits, it now could be possible to control the distribution of flow into multiple fractured zones using in-well flow control methods, such as by limiting the size of perforations through the casing of the wells to impose a higher backpressure. Increased backpressure helps to equalize flow from one fracture to the next in a simple way that does not require complex high-temperature tolerant tools. We note that increasing backpressure by this method is incompatible with standard (i.e., non caged) seismicity mitigation procedures because there is no way to prevent injection pressure limits from being exceeded when using limited-size perforations. Combining this ability to better control flow distribution with the improved heat transfer efficiency of sheet-like flow offers a two-prong benefit towards delaying the onset of cooling. Thus, fracture caging could be a solution to not only reducing seismic risk (1) and better optimizing flow rates (2), caging could also be a solution to delaying the onset of cooling in the production wells (3).

Much more work is needed before caging can become a deployed tool to better control fluid flow for geothermal systems. Furthermore, it does not escape our notice that caging could also have a future role in oil and gas, hydrogen storage, saltwater disposal, nuclear waste disposal, superfund site contaminant treatment, and carbon sequestration applications. This study serves as a step in an effort to improve the robustness of our energy economy. Future work on this topic will benefit from contributions from the greater scientific and technical community.

6 Conclusions

These results from our model and experiments reveal crucial information about the feasibility of fracture caging for enhanced geothermal systems (EGS). First, the experiments unequivocally prove that boundary wells can halt hydraulic fracture growth. Second, the experiments prove that a caged fracture can be held open with high-pressure fluid without inducing fracture growth. This presents hydropropping as a feasible alternative to injecting solid proppant particles or relying on shear asperity propping to maintain fracture permeability. Third, the model and experiments demonstrate that fracture caging has an upper flow rate limit, above which fractures will resume growth (Fig. 2 and Fig. 8). The model predicts two domains to this limit. At close well spacing as was used in the experiments, fracture conductivity dominates the injection rate limit. At larger well spacing as is appropriate to commercial EGS, the maximum caged injection rate is dominated by frictional flow losses through the wells. Increasing well diameter enables faster injection rates to be caged. Fourth, the experiments demonstrate that unstable fracture caging will occur with two or fewer boundary wells. Stable fracture caging is demonstrated to require three of more wells. This result is important for economics since geothermal wells are very expensive and our companion work predicts that caged EGS could be economic with three boundary wells [Frash et al., 2023]. Fifth, this work demonstrates the importance of stimulating fractures perpendicular to the wells, whether by notching, perforating, or exploiting the in-situ stress state. A hydraulic facture that bypasses all the wells in a cage will obviously cause caging to fail. Sixth, even when a hydraulic fracture is not caged a large fraction of the injected fluid can be recovered from the boundary wells. Seventh, our model to predict the limits of fracture caging is simplistic so new advanced models would be beneficial for more fully exploring the limits of fracture caging, especially with respect to the effects of porous rock, shear fracture activation, and the interplay between caging and seismic risk. Eighth, our AE measurements reinforce the notion that microseismic data is unreliable for monitoring fracture growth yet is still better than nothing since AE activity often coincides with fracture growth. Overall, this work presents not a small step, but rather a leap forward in validating fracture caging and hydropropping as tools to improve the control of fluid flow and fracture growth in the subsurface.

Acknowledgments

This work is supported by Department of Energy (DOE) Basic Energy Sciences under FWP LANLE3W1. Additional support was provided by Los Alamos National Laboratory's Laboratory Directed Research and Development – Exploratory Research program under LDRD-ER-20220175ER. We are grateful for the funding provided by DOE and LANL.

Open Research

Data including timeseries, videos, and our model's script in the Python language can be accessed freely at https://zenodo.org/record/8274273 (doi: 10.5281/zenodo.8274273).

References

André, L., Rabemanana, V., & Vuataz, F.D. (2006). Influence of water–rock interactions on fracture permeability of the deep reservoir at Soultz-sous-Forêts, France. Geothermics, 35(5-6), 507-531.

Catalli, F., Meier, M.A., &Wiemer, S., (2013). The role of Coulomb stress changes for injection-induced seismicity: The Basel enhanced geothermal system. *Geophysical Research Letters*, 40(1), 72-77.

Cuenot, N., Dorbath, C., & Dorbath, L. (2008). Analysis of the microseismicity induced by fluid injections at the EGS site of Soultz-sous-Forêts (Alsace, France): implications for the characterization of the geothermal reservoir properties. *Pure and Applied Geophysics*, 165(5), 797-828.

Detournay, E. (2004). Propagation Regimes of Fluid-Driven Fractures in Impermeable Rocks. International Journal of Geomechanics, 4(1): 35-45.

Ellsworth, W.L. (2013). Injection-induced earthquakes. *Science,* 341(6142), 1225942.

Frash, L.P., (2022). Optimized Enhanced Geothermal Development Strategies with GeoDT and Fracture Caging. Paper presented at 47th Workshop on Geothermal Reservoir Engineering, Stanford University, Stanford, CA.

Frash, L.P., Carey, J.W., Ahmmed, B., Men, M., Sweeney, M., K C, B., and Iyare, U. (2023) A proposal for profitable enhanced geothermal systems in hot dry rock. Paper presented at 48th Workshop on Geothermal Reservoir Engineering, Stanford, CA, USA, February 6-8,

Frash, L.P., Fu, P., Morris, J., & EGS Collab Team, (2018). Fracture caging: Can we control the extent of a hydraulic fracture stimulated zone. Paper presented at 43rd Workshop on Geothermal Reservoir Engineering, Stanford University, Stanford, CA.

Frash, L.P., Fu, P., Morris, J., Gutierrez, M., Neupane, G., Hampton, J., Welch, N.J., Carey, J.W., & Kneafsey, T. (2021). Fracture caging to limit induced seismicity. *Geophysical Research Letters*, 48(1), p.e2020GL090648.

Frash, L.P., Gutierrez, M., Hampton, J., & Hood, J. (2015). Laboratory simulation of binary and triple well EGS in large granite blocks using AE events for drilling guidance. *Geothermics*, 55: 1-15.

Fu, P., Schoenball, M., Ajo-Franklin, J.B., Chai, C., Maceira, M., Morris, J.P., Wu, H., Knox, H., Schwering, P.C., White, M.D., &Burghardt, J.A. (2021). Close observation of hydraulic fracturing at egs collab experiment 1: Fracture trajectory, microseismic interpretations, and the role of natural fractures. *Journal of Geophysical Research: Solid Earth*, 126(7), p.e2020JB020840.

Galis, M., Ampuero, J.P., Mai, M., Cappa, F. (2017). Induced seismicity provides insight into why earthquake ruptures stop. *Science Advances*, 3, eeap7528.

Garcia, J., Hartline, C., Walters, M., Wright, M., Rutqvist, J., Dobson, P.F., & Jeanne, P. (2016). The Northwest Geysers EGS demonstration project, California: Part 1: characterization and reservoir response to injection. *Geothermics*, 63, 97-119.

Gee, B., Gracie, R., & Dusseault, M.B. (2021). Multiscale short-circuiting mechanisms in multiple fracture enhanced geothermal systems. *Geothermics*, 94, 102094.

Gringarten, A.C., Witherspoon, P.A., Ohnishi, Y. (1975). Theory of heat extraction from fractured hot dry rock. *Journal of Geophyscial Research*, 80, 1120-1124.

Hamm, S.G., Augustine, C.R., Tasca, C., & Winick, J. (2019). *An Overview of the US Department of Energy's GeoVision Report*. Golden, CO: National Renewable Energy Laboratory.

Hu, L., Ghassemi, A. (2017). Characterization of Hydraulically Induced Fracture in Lab-scale Enhanced Geothermal Reservoir. *GRC Transactions*, 41.

Ito, T., & Zoback, M. D. (2000). Fracture permeability and in situ stress to 7 km depth in the KTB scientific drillhole. *Geophysical Research Letters*, 27, 1045–1048.

Jeanne, P., Rutqvist, J., Rinaldi, A.P., Dobson, P.F., Walters, M., Hartline, C., & Garcia, J. (2015). Seismic and aseismic deformations and impact on reservoir permeability: The case of EGS stimulation at The Geysers, California, USA. *Journal of Geophysical Research: Solid Earth*, 120(11), 7863-7882.

Jeppson, R.W. (1974) Steady flow analysis of pipe networks: an instructional manual. *Reports*, Paper 300.

Kanamori, H. and Anderson, D.L. (1975). Theoretical basis of some empirical relations in seismology. *Bulletin of the seismological society of America*, 65(5), 1073-1095.

Katende, A., Allen, A., Massion, C., Awejori, G., Xiong, F., Radonjic, M., Rutqvist, J., Nakagawa, S. (2022). Experiments and modeling of proppant embedment and fracture conductivity for the Caney Shale, Oklahoma, USA. Paper presented at 56th U.S. Rock Mechanics/Geomechanics Symposium, Santa Fe, NM, USA, June.

Kelkar, S., WoldeGabriel, G., & Rehfeldt, K. (2016). Lessons learned from the pioneering hot dry rock project at Fenton Hill, USA. *Geothermics*, 63, 5-14.

Kim, K.H., Ree, J.H., Kim, Y., Kim, S., Kang, S.Y., & Seo, W. (2018). Assessing whether the 2017 M w 5.4 Pohang earthquake in South Korea was an induced event. *Science*, 360(6392), 1007-1009.

Majer, E., Nelson, J., Roberson-Tait, A., Savy, J., Wong, I. (2012). Protocol for addressing induced seismicity associated with enhanced geothermal systems. *US Department of Energy: Geothermal Technologies Program*.

Meng, M., Frash, L.P., Li, W., Welch, N.J., Carey, J.W., Morris, J., Neupane, G., Ulrich, C., & Kneafsey, T. (2022). Hydro-Mechanical Measurements of Sheared Crystalline Rock Fractures With Applications for EGS Collab Experiments 1 and 2. *Journal of Geophysical Research: Solid Earth*, 127(2), e2021JB023000.

Ohtsu, M. (1991). Simplified moment tensor analysis and unified decomposition of acoustic emission source: application to in situ hydrofracturing test. *Journal of Geophysical Research: Solid Earth*, 96(B4), 6211-6221.

Ohtsu, M. (1995). Acoustic emission theory for moment tensor analysis. *Research in Nondestructive Evaluation*, 6(3), 169-184.

Okoroafor, E.R., Co, C., Horne, R.N. (2022). Numerical investigation of the impact of fracture aperture anisotropy on EGS thermal performance. *Geothermics*, 100, 102354.

Petrovich, C.L., Nolte, D.D., Pyrak-Nolte, L.J. (2013). Scaling of fluid flow versus fracture stiffness. *Geophysical Research Letters*, 40, 2076-2080.

Petty, S., Nordin, Y., Glassley, W., Cladouhos, T.T., & Swyer, M. (2013). Improving geothermal project economics with multi-zone stimulation: results from the Newberry Volcano EGS demonstration. Paper presented at Proceedings of the Thirty-Eighth Workshop on Geothermal Reservoir Engineering, Stanford University, Stanford, CA.

Pruess, K. (2008). On production behavior of enhanced geothermal systems with CO_2 as working fluid. *Energy Conversion and Management*, 49(6), 1446-1454.

Sneddon I., Lowengrub M. (1969) Crack Problems in the Classical Theory of Elasticity, The SIAM series in Applied Mathematics, John Wiley & Sons.

Tester, J., Andersen, B.J., Batchelor, A.S., Blackwell, D.D., DiPippo, R., Drake, E.M., Livesay, B., Morre, M.C., Nichols, K., Petty, S. (2006). The Future of Geothermal Energy. *Massachusetts Institute of Technology*, ISBN: 0-615134386.

Valko, P., Economides, M.J. (1996). *Hydraulic Fracture Mechanics*. Wiley, 320p.

Weerasooriya, T., Moy, P., Casem, D., Cheng, M., Chen, W. (2006). Fracture Toughness for PMMA as a Function of Loading Rate. Paper presented at the 2006 SEM Annual Conference and Exposition on Experimental and Applied Mechanics.

Welch, N.J., Carey, J.W., Frash, L.P., Hyman, J.D., Hicks, W., Meng, M., Li, W., Menefee, A.H. (2022). Effect of shear displacement and stress changes on fracture hydraulic aperture and flow anisotropy. *Transport in Porous Media*, 141, 17-47.

Witherspoon, P.A., Wang, J.S.Y., Iwai, K., Gale, J.E. (1980). Validity of cubic law for fluid flow in a deformable rock fracture. *Water Resources research*, 16: 1016-1024.

Yen, R.T. (1962). Radial flow between two parallel discs. *A Master's Report*: *Kansas State University*, Department of Applied Mathematics.

Zoback, M.D., Gorelick, S.M. (2012). Earthquake triggering and large-scale geologic storage of carbon dioxide. *PNAS*, 109(26), 10164–10168.

Tables and Figures

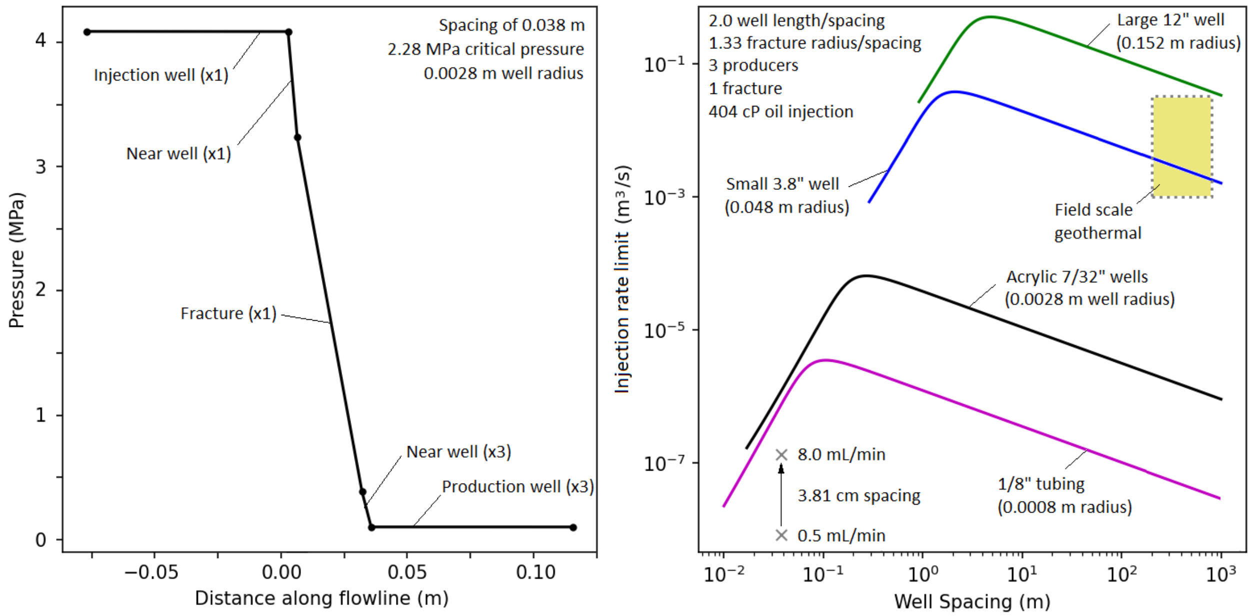

Fig. 1. Our analytical model’s prediction of caging across dimensional scales. (Left) Pressure profile with flow through the injection-well, near-injection-well, fracture, near-production-wells, and production-wells. In this case, pressure losses are dominated by the fracture in laboratory-scale experiments unless the boundary wells are choked. (Right) Maximum caged injection rate limit as a function of well spacing and well radius. The shaded box in the upper right highlights the well spacing and flow rates needed for full-scale enhanced geothermal systems. Two ×’s mark the lower and upper flow rates in our laboratory experiments.

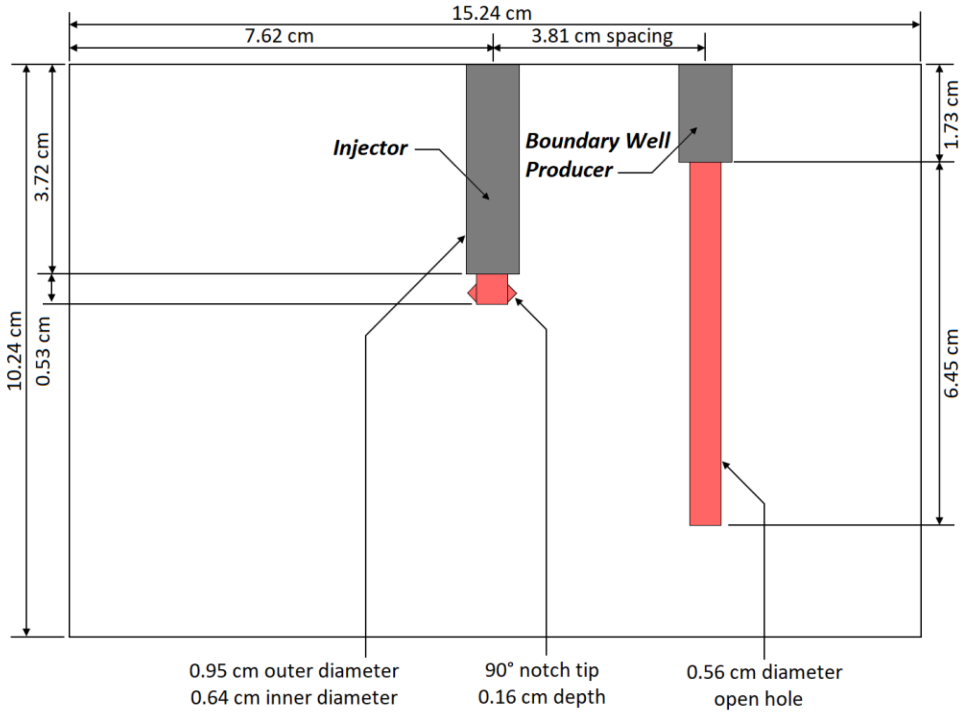

Fig. 2. Nominal dimensions of the hydraulic fracture experiments.

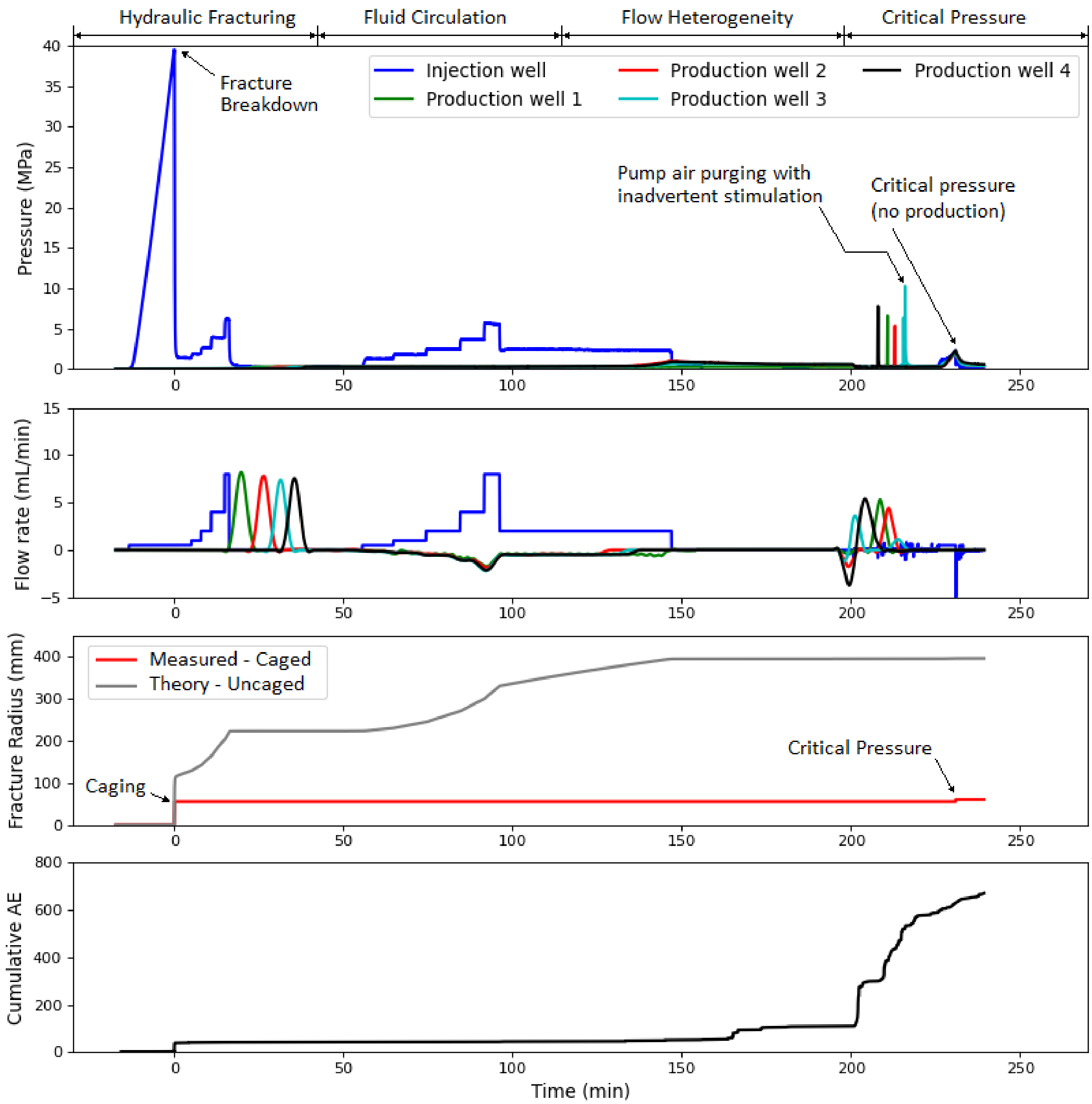

Fig. 3. Timeseries of fracture caging with four boundary wells and 50 mL of air in each boundary pump to accommodate the hydraulic fracture breakdown's flow surge. Plotted data includes a theoretically predicted fracture radius for an uncaged fracture in the same acrylic material as a function of measured injected volume with a nominal net pressure of 2.3 MPa. Measured fracture growth and acoustic emissions were negligible after the fracture was caged at 0.13 min (7.7 s). Later in the experiment at 217 and 231 min fracture propagation was induced by injecting without production to measure the 2.28 MPa critical pressure for propagation. Acoustic emissions occurred during fracture propagation and heterogeneous flow.

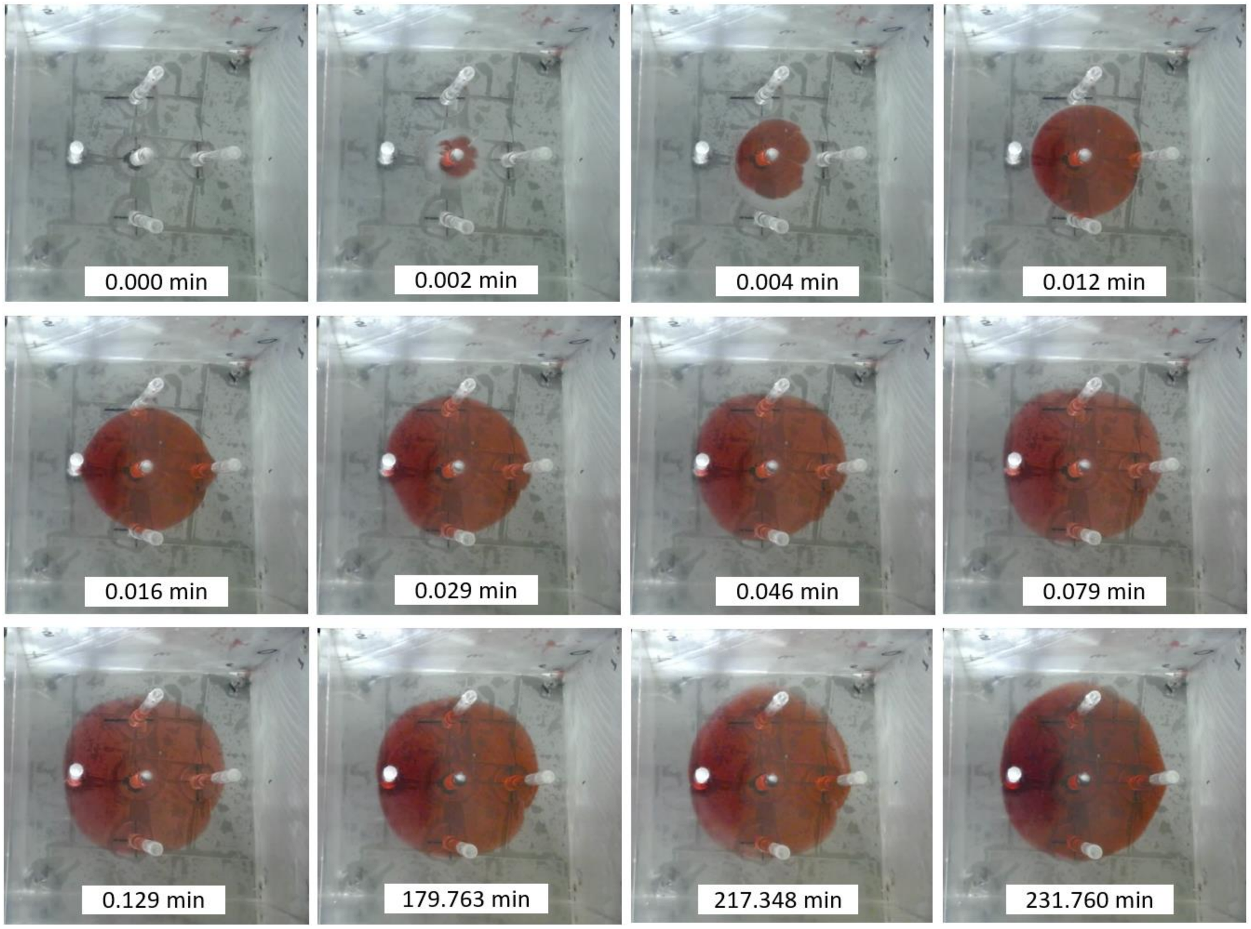

Fig. 4. Placing four boundary producers around the injector enabled successful caging during hydraulic fracturing (0.000 < t < 50 min), fluid circulation at 0.5 to 8.0 mL/min (50 < t < 120 min), and heterogeneous flow (120 < t < 200 min). Injection without production measured a critical pressure of 2.3 MPa for renewed fracture growth. This result unequivocally demonstrates that hydraulic fracture growth can be halted by a cage of boundary wells and that a fracture can be stably hydropropped for fluid circulation at high net pressures without solid proppants nor shear stimulation. Video of our experiments can be accessed from our online data repository (https://zenodo.org/record/8274273).

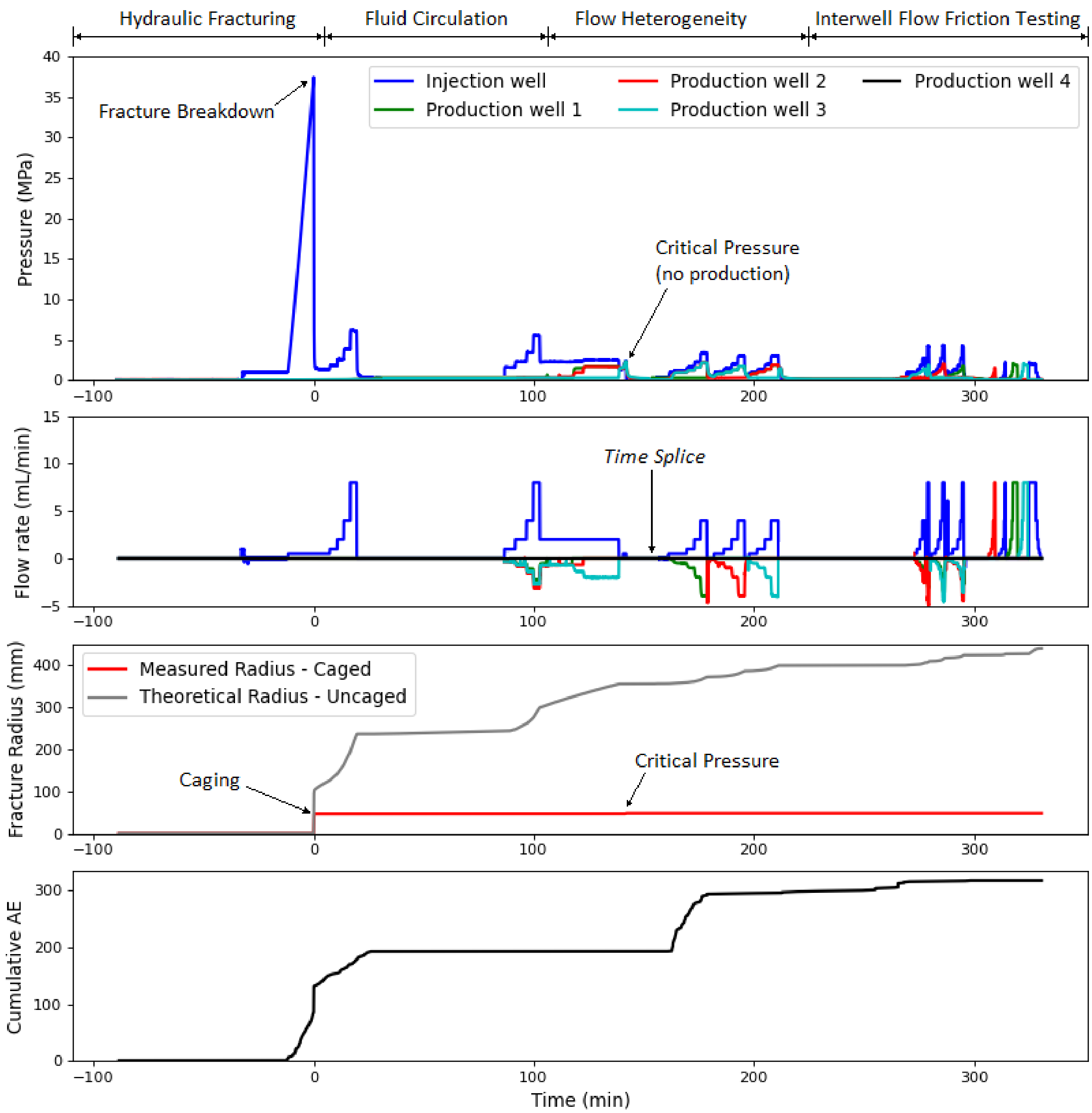

Fig. 5. Timeseries of fracture caging with three boundary wells and 50 mL of air in each boundary pump to accommodate the hydraulic fracture breakdown's flow surge. Measured fracture growth and acoustic emissions were negligible after the fracture was caged at 0.18 min. Later in the experiment at 140 min fracture propagation was induced by injecting without production to measure the 2.3 ± 0.1 MPa critical pressure for propagation.

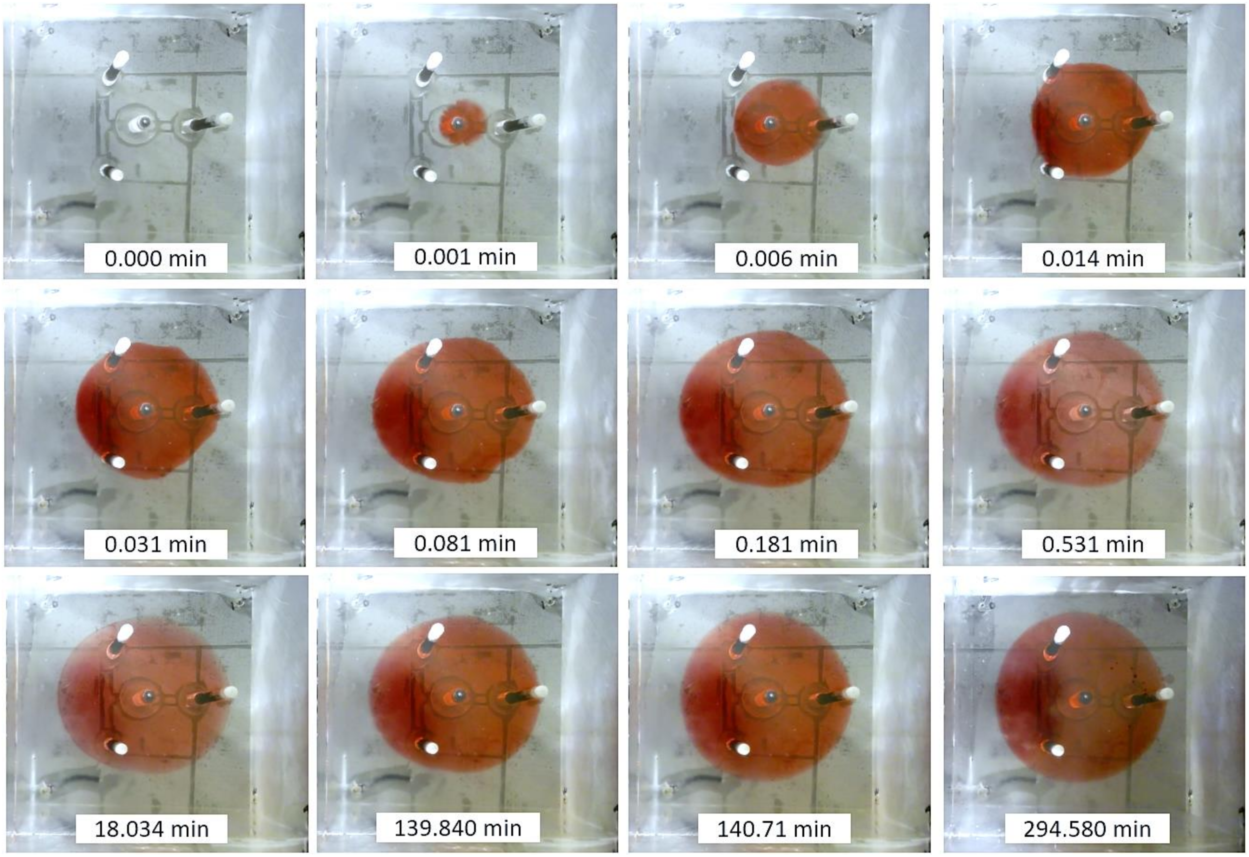

Fig. 6. Placing three boundary producers around the injector enabled successful caging during hydraulic fracturing (0.000 < t < 18 min), fluid circulation (18 < t < 105 min), and heterogeneous flow (145 < t < 300 min). Injection without production measured a critical pressure of 2.3 MPa for renewed fracture growth (i.e., 140 min).

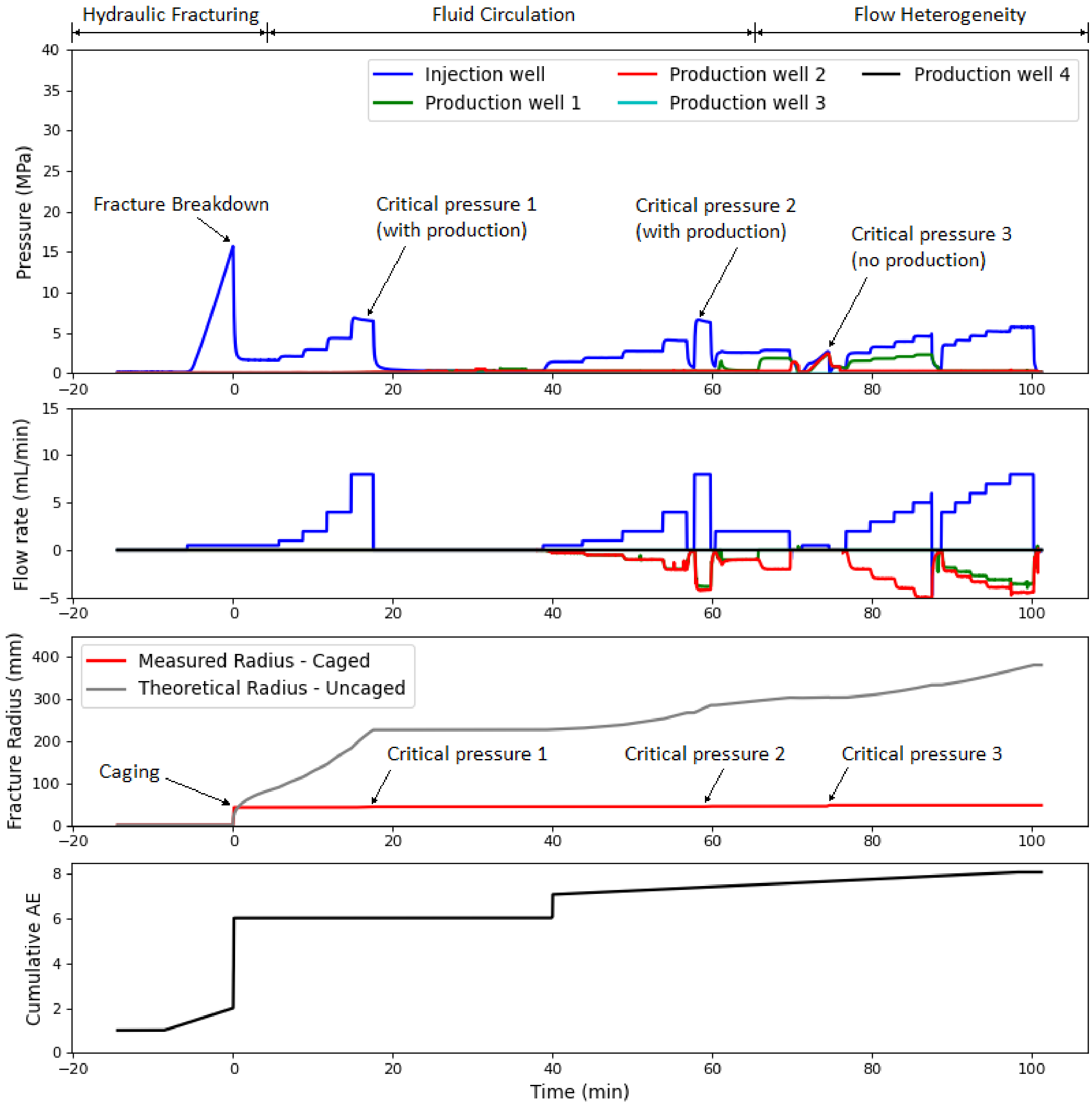

Fig. 7. The two-producer pattern did successfully cage, but this cage was less stable than the three-producer and four-producer alternatives. This instability was evident from fracture growth at 8.0 mL/min injection. Asymmetry in the caged fracture is another indicator of instability (c.f., Fig. 8). Fracture growth was induced by high circulation rates at 16 min and again at 59 min. Stable injection-only growth was induced with 0.5 mL/min injection at 74 min. After each period of fracture growth, the fracture was observed to become more stable until 8.0 mL/min was eventually accommodated without fracture growth. This result agrees with our model in that increasing fracture radius improves cage effectiveness.

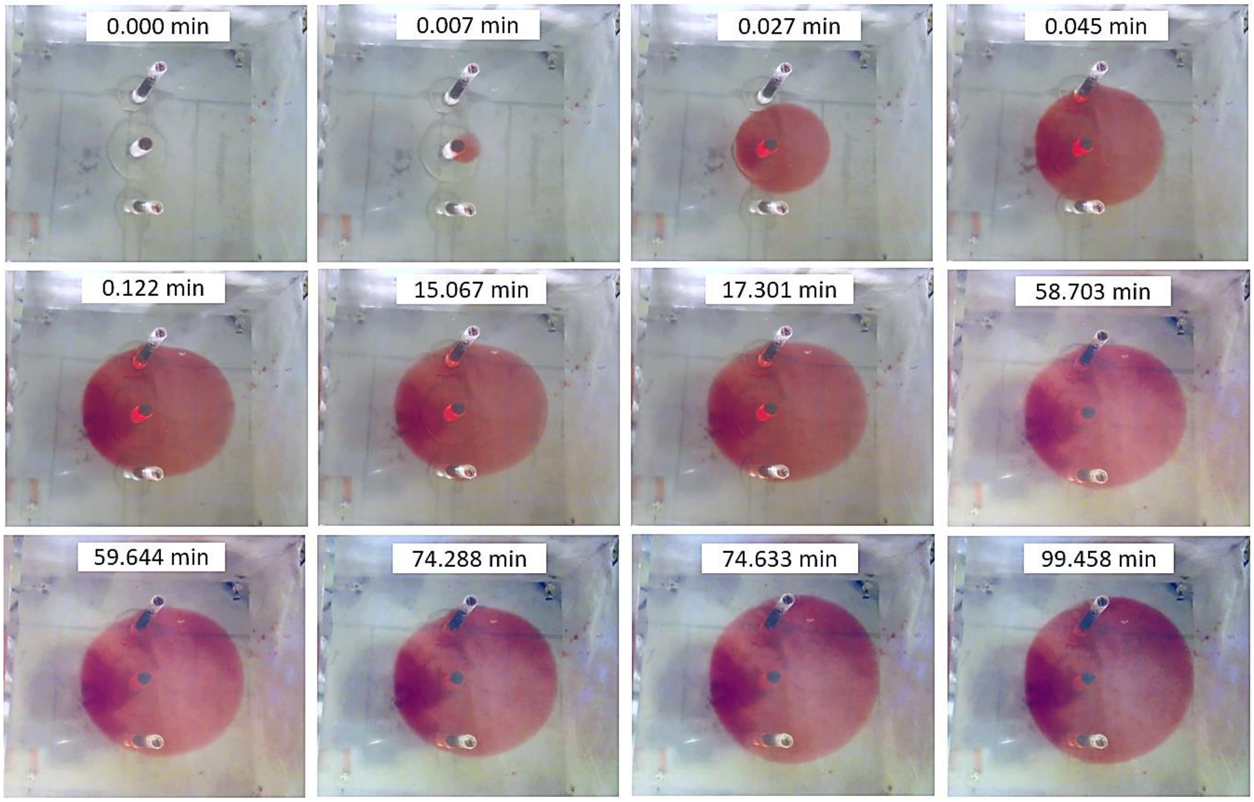

Fig. 8. Fracture caging with two boundary wells was unstable during fluid circulation because fracture propagation reinitiated during 8 mL/min injection at 16 min and 59 min, despite the simultaneous fluid production. At its largest radius after the critical pressure test at 74 min, the fracture finally became more stable and able to accommodate fluid circulation at 8 mL/min without growing. This validates the analytical model's prediction that higher flow rates can be caged as a fracture grows larger.

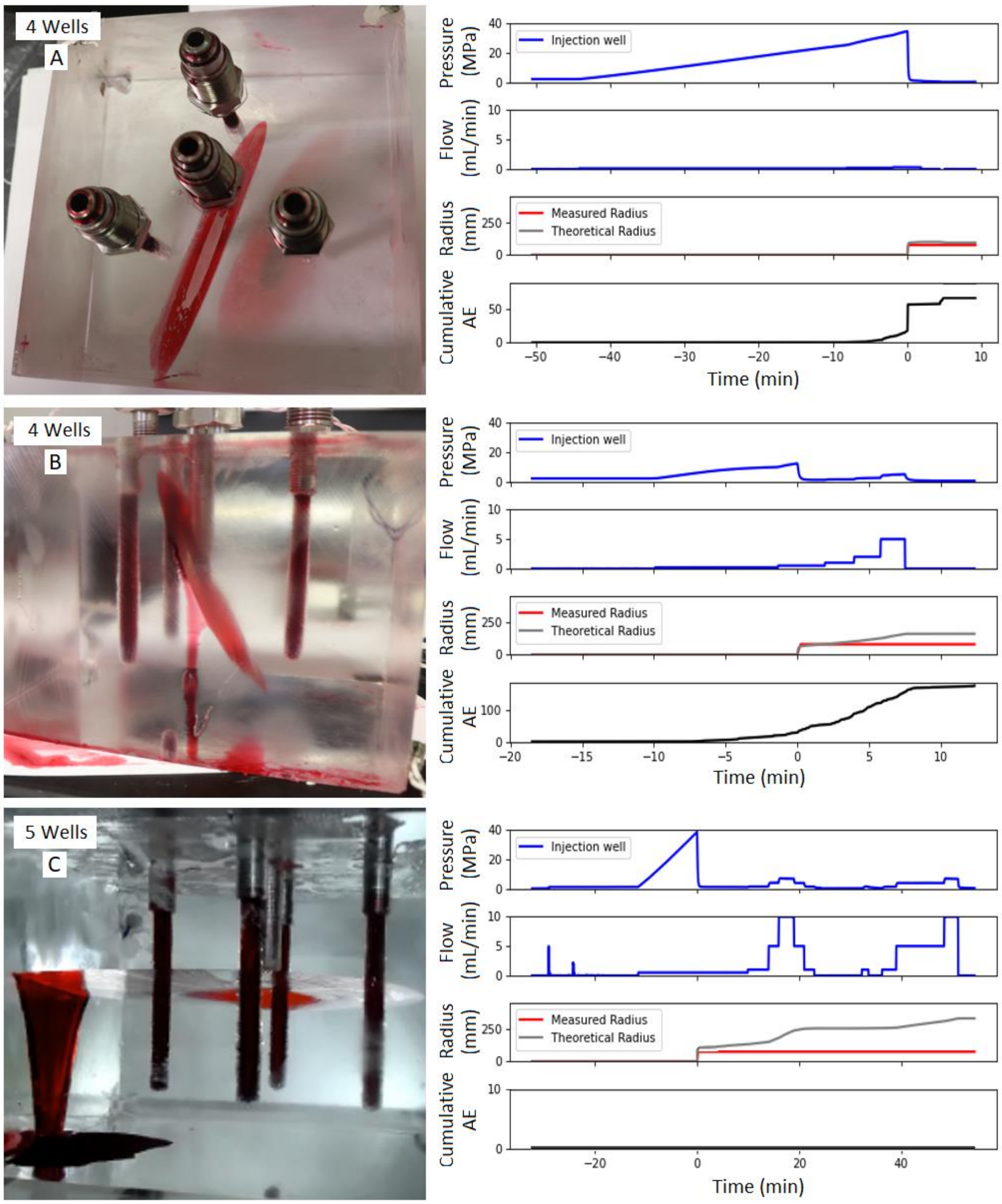

Fig. 9. Scenarios demonstrating uncaged hydraulic fractures. These hydraulic fractures reached the outer edge of the block because of (A) entirely missing the boundary wells or (B and C) the boundary wells flowing too slowly to contain the fractures. Unlike the caged experiments, the boundary wells and pumps in these cases were bled of air to minimize hydraulic compliance. These scenarios show the importance of accommodating the surge in flow that occurs when the hydraulic fracture first intersects each boundary well.